23. Huyghe, P., Galy, A., Mugnier, J. L. and France-Lanord, C., Propagation of the thrust system and erosion in the Lesser Himalaya: Geochemical and sedimentological evidence. *Geol. Soc. Am. Bull.*, 2001, **29**, 1007–1010.
24. Lawson, A. C., Isostatic compensation considered as a cause of thrusting. *Geol. Soc. Am. Bull.*, 1922, **33**, 337–351.
25. Moore, G. F., Shipley, T. H. and Lonsdale, P. E., Subduction erosion versus sediment offscraping at the toe of the Middle American Trench off Guatemala. *Tectonics*, 1986, **5**, 513–523.

ACKNOWLEDGEMENTS. We thank Prof. M. P. Singh, Head, Department of Geology, University of Lucknow for providing working facilities and for constant encouragement. We also thank Prof. I. B. Singh for fruitful discussion. This work is part of a DST project awarded to K.K.A. Financial assistance to G.K.A. by CSIR is acknowledged.

Received 8 July 2003; revised accepted 17 March 2004

Development of single-molecule tracking confocal microscope combined with force spectroscopy for gene-expression analysis

Deepak Kumar Sinha[1], Dipanjan Bhattacharya[2], Bidisha Banerjee[1], Feroz Meeran Hameed[1] and G. V. Shivashankar[1,2,*]

[1]National Centre for Biological Sciences, Tata Institute of Fundamental Research, GKVK Campus, Bangalore 560 065, India
[2]Raman Research Institute, C.V. Raman Avenue, Bangalore 560 080, India

We have constructed a confocal fluorescence microscope combined with force measurements. Our method allows for simultaneous measurements of fluorescence anisotropy, energy transfer and correlation. The methodology and the sensitivity of the set-up using enhanced green fluorescent protein are described. We present results on (a) the detection of mRNA polymerization during *in vitro* transcription using fluorescence correlation spectroscopy and anisotropy, (b) detection of *in vivo* protein-DNA interactions using fluorescence anisotropy and (c) nanomanipulation of polytene chromosomes using the micropippete force sensor. Such a combined method allows for probing novel structure–function relationship underlying gene-expression.

RECENT progress in single-molecule force and fluorescence detection[1–3] has opened new possibilities in the area of nanobiology. Typical sensitivity in these measurements is in the range of femtonewton forces[4] and subnanomolar concentrations[3]. The ability to manipulate and detect single-molecules provides a handle to probe the subtle relation among structure, function and dynamics of biomolecules and their interactions. In addition, such methods are finding increasing analytical applications, for example, in sorting and counting of single-molecules, rare-event detection, probe–target binding, high throughput screening, imaging of cells and single-molecule DNA sequencing[5–8]. In the above fluorescence-based studies, a number of specific methods (such as fluorescence correlation spectroscopy (FCS), anisotropy, energy transfer and lifetime techniques) have been used with some advantages and disadvantages. For example, in FCS when analysing heterogeneous molecule ensemble samples, the sampling of multiple events results in ensemble averaging and hence an integrated method using both energy-transfer and anisotropy of molecules would provide a more quantitative method. The intensity and anisotropy recorded at fast binning time (as low as 100 ns) can be used to resolve different conformations and conformational fluctuations of single-molecules. Therefore, a combined experimental set-up that incorporates various fluorescence methods provides a powerful tool to investigate single biomolecular interactions and their dynamics. In addition, its integration to a force sensor allows one to tune the biomolecular structure–function relationship.

Here we describe the development of a confocal fluorescence microscope with fluorescence correlation and anisotropy tracking combined with sensitive micropippete force sensor. We present experiments to address the biophysical aspects of gene-expression that illustrate the importance of the above methods. In particular, we show (a) the detection of mRNA polymerization during *in vitro* transcription using fluorescence anisotropy and correlation spectroscopy, (b) detection of *in vivo* protein–DNA interactions using fluorescence anisotropy and (c) nanomanipulation of polytene chromosomes using the micropipette force sensor.

Figure 1 is a schematic of our experimental set-up. An inverted optical microscope (model IX 70; Olympus, Japan) is placed on a vibration isolation table (model 63–573; Technical Manufacturing Corporation, Peabody, MA, USA). The instrument incorporates an Ar-ion laser (model 163-D0105, 125 mW; Spectra-Physics, Mountain View, CA, USA) for the excitation of the sample. Neutral density (ND) filters (model NDK01; ThorLabs, Newton, NJ, USA) fitted on a filter wheel (model FW2A; ThorLabs) in front of the laser are used to attenuate the power of the laser when so desired. The laser beam diameter is expanded from 0.7 to 4.2 mm using the appropriate lens combination to minimize the focal diameter in the object plane. The beam is passed through a polarizer (model 03 FPG 001, dichroic sheet polarizer; Melles Griot, Rochester, NY, USA) before being passed into the microscope. The laser emits in three wavelengths – 458, 488 and 514 nm. The 488 nm laser line is selected using an excitation filter (model HQ480/40x; Chroma, Brattleboro, VT, USA) fitted in the filter cube (model UMF2; Olympus) of the micro-

*For correspondence. (e-mail: shiva@ncbs.res.in)

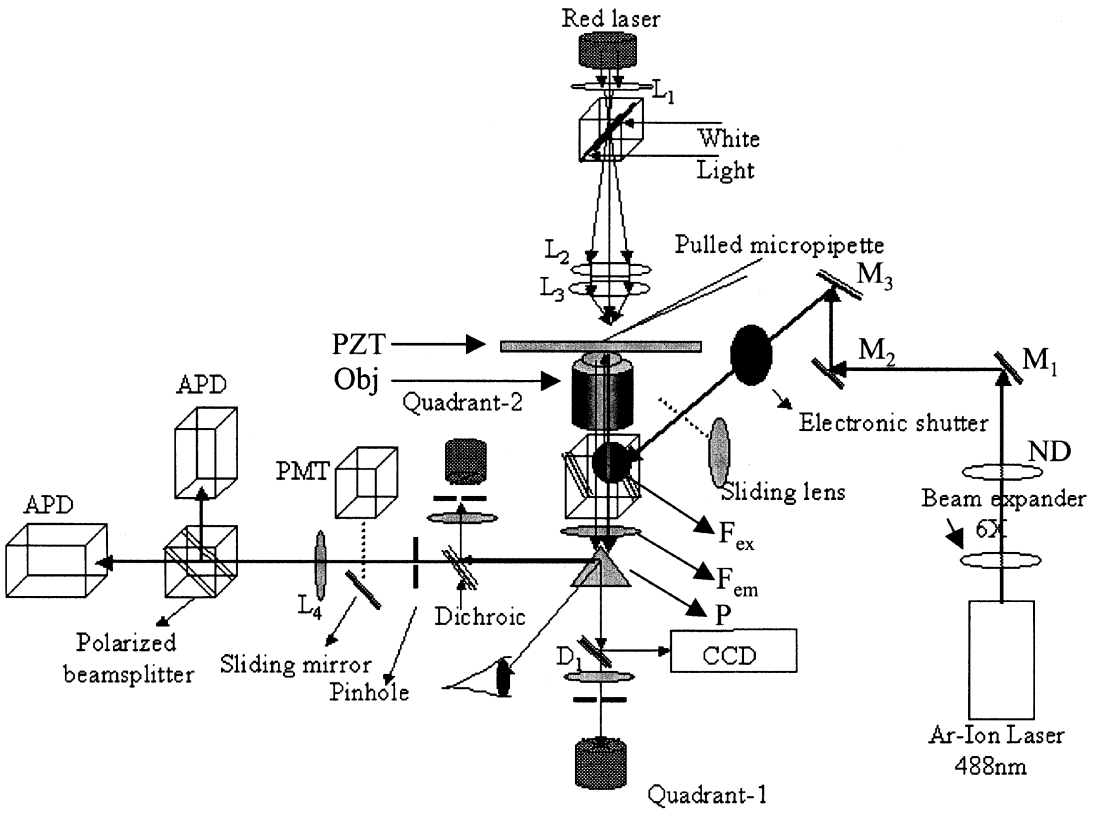

Figure 1. Schematic of the experimental set-up. D, Dichroic mirror; F_{em}, Emission filter; F_{ex}, Excitation filter; L_1, L_2, L_3, L_4, Focussing lens; M_1, M_2, M_3, Mirrors; Obj, Objective (100 ×/1.4 NA), ND, Neutral density filter; P, Microscope prism; PMT, Photomultiplier tube; PZT, Nanometre precision 3-axis piezoelectric transducer stage; APD, Avalanche photodiode.

scope. The laser beam is reflected to the objective (100×, 1.4 NA, oil immersion; Olympus) using a dichroic mirror (model DM500; Olympus) fitted in the cube. Using a sliding lens (f = 300 mm, to focus in the back focal plane of the objective) in the laser path, we can get a Kohler illumination for fluorescence visualization of the complete field of view.

Precise movement of the sample with respect to the confocal spot is achieved using a nanometre-precision three-axis piezo-electric transducer (PZT) stage (range 100 μm × 100 μm × 20 μm, model 547.3CL; Physik Instrumente, Waldbronn, Germany) controlled by a LVPZT amplifier module (model E-503.00; Physik Instrumente) with a Position servo controller (model E-509.C3; Physik Instrumente) and a PZT displacement display (model E-515.03; Physik Instrumente). The Position controller is interfaced to the computer through a shielded BNC connector board (model BNC-2090; National Instruments, Austin, TX, USA) connected to a 16-bit data acquisition (DAQ) board (PCI-MIO-16XE-10; National Instruments). Coarse movement of the sample is provided by a manual two-axis microscope stage (IX-MVR; Olympus). Coarse movement on the third axis is provided by the focusing controls of the objective.

For force measurement, micropipettes (force cantilevers) are pulled from borosilicate glass capillaries (BF120-94-10; Sutter Instrument Company, Novato, CA, USA) using a pipette puller (horizontal puller, model P-97; Sutter Instrument Company). The pulling is optimized to consistently give us micropipettes with tip size of about 0.5 μm and taper length of a centimetre. The micropipette is coated with 30 nm of gold using a sputtering machine with a film thickness monitor (model sputter coater 108 auto; Pelco International; Redding, CA, USA). After coating, the micropipette is fixed onto a micromanipulator (right-handed motorized micromanipulator with remote, model DC3001; World Precision Instruments Inc., Sarasota, FL, USA). The micromanipulator allows the micropipette to be positioned relative to the fluorescence excitation and the red laser in the sample plane. The light beam from a red laser (635 nm, 5 mW power, model 31-0128; Coherent, Auburn, CA, USA) is expanded using a combination of two lenses (aspheric lens, f = 4.5 mm, model C230TM; ThorLabs, and planoconvex lens, f =100 mm, model BPX075; ThorLabs). A third lens (planoconvex lens, f = 50 mm, model BPX060; ThorLabs) is used to focus the beam onto the pipette. The forward scatter from the pipette is collected through the

objective and used to image the pipette on the quadrant detector (QD; four-element, segmented photodiode, model SPOT-4DMI; UDT sensors, Hawthorne, CA, USA). An iris is used in front of the quadrant detector to block all ambient scattered light and thereby improve the signal-to-noise ratio. The output currents from the four segments are fed into a quadrant amplifier (model 431 X-Y Position Indicator; UDT Instruments, Baltimore, MD, USA). The voltage output from the amplifier (a measure of the position of the micropipette tip) is fed into the computer through the data acquisition board. The displacement of the micropipette tip, which gives us the bending of the micropipette, is used to calculate the force exerted by the micropipette. The custom-made micropipettes, whose stiffness can be tuned by the fabrication process, offer a flexible alternative to atomic force cantilevers. Bright field imaging in transmission mode is achieved using a fibre-optic microscope lamp (model PL-900; Dolan-Jenner, Lawrence, MA, USA). A CCD camera (model XC-77CE; Sony, Japan) attached to the camera port of the microscope is used to acquire images, display it on a TV monitor (model KV-B14PD1; Sony), recorded on a videotape through a video cassette recorder (model VC-MA33; Sharp, Japan) or digitized onto the computer using an image acquisition card (IMAQ card, model PCI-1411; National Instruments).

The fluorescence collected from the sample through the objective lens is reflected to the side port using the microscope optics. A 50 μm pinhole (model P50S; ThorLabs) is used to section the image plane. The pinhole is mounted on a XYZ stage (model 460P-XYZ; Newport Corporation, Irvine, CA, USA) with three motorized actuators (model 850G; Newport Corporation) connected to a three-axis motion controller (model ESP 300-111N2; Newport Corporation) interfaced to the computer through the RS-232 interface. Light passing through the pinhole is focused on the avalanche photodiodes (APDs; single photon counting modules, model SPCM-AQR-14; Perkin Elmer, Fremont, CA, USA) by a biconvex lens (f = 35 mm, model LB1811-B; ThorLabs). Prior to this, the beam is passed through an emission filter (HQ535/50 m; Chroma), to remove all the wavelengths other than the emission band of the fluorescent molecule, and split into its polarized components using a polarizing beamsplitter (model 5811; New Focus, Santa Clara, CA, USA). The APDs are powered by a DC power supply (triple output DC power supply, model 3630A; Agilent, Palo Alto, CA, USA). The outputs from the APDs are used for correlation measurements by connecting them to the correlator board (model Flex99R-480; Correlator.com, Bridgewater, NJ, USA), or sampled at a fast timescale using a dual channel gated photon counter (model SR400; Stanford Research Systems, Sunnyvale, CA, USA) gated with a function generator (30 MHz Function and Arbitrary Waveform Generator, model DS345; Stanford Research Systems), or counted at a low time bin using the DAQ board. The correlator board and the dual channel photon counter are interfaced to the computer using the USB and RS-232 interface respectively. A movable mirror, which can reflect light on to a photomultiplier tube (model P10PC; Electron Tubes, Rockaway, NJ, USA), is used to align the pinhole. For simultaneous force measurements, a dichroic (model 580DCSP; Chroma) is used to reflect the forward scatter of the red laser projected on the pipette, while the fluorescence light is transmitted to the pinhole (Figure 1).

In Figure 2, a typical intensity time series is shown to illustrate the detection of single-molecules passing through the confocal volume. Figure 2 *a* shows the linear dependence in fluorescence intensity to the sample concentration down to sub-nanomolar concentration. In Figure 2 *b* we plot the typical correlation function of enhanced green fluorescent protein (EGFP) molecules using FCS[3]. The correlation function $G(t)$ is defined as

$$G(t) = \frac{\langle F(t)F(t+t)\rangle}{\langle F(t)^2\rangle},$$

where $F(t)$ is the fluorescence intensity measured at time t. To obtain the diffusion timescales of EGFP, the data were fitted to

$$G(t) = \frac{1}{N\left(1+\frac{t}{t_D}\right)\sqrt{\left(1+\frac{t}{t_{Dz}}\right)}}+1,$$

where $G(t)$ is the theoretical correlation function for freely diffusing molecules in 3D, N the average number of fluorophores in the confocal volume, t_D the resident time in the confocal volume along the XY plane and t_{D_z}

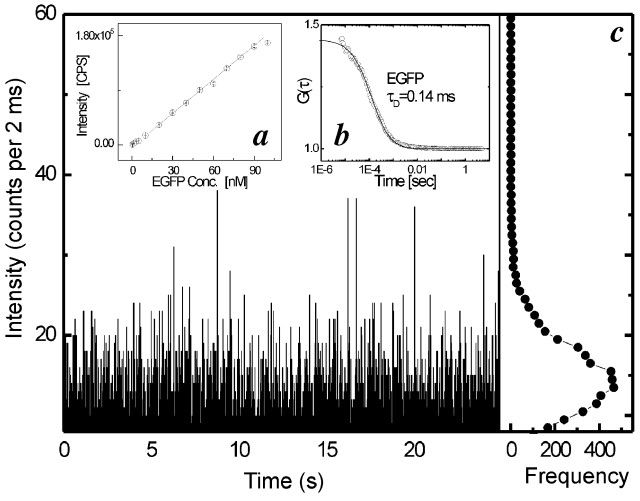

Figure 2. Plot of a typical time series of EGFP intensity measured resolving individual molecular events. ***a***, Plot of mean counts at varying concentration of EFGP; ***b***, Typical correlation function of EGFP. ***c***, Histogram of the counts of the time series.

the resident time in the confocal volume along the *Z*-axis, which defines the correlation in a confocal volume. From the fit, the $G(0)$ value (which is a measure of the average number of fluorescent particles in the confocal volume) and t_D ($w^2 = 4Dt_D$, where w is the $1/e^2$ radius of the confocal spot and D the diffusion constant) are obtained. t_D for EGFP is obtained as 0.14 ms.

The sensitivity of the anisotropy[9] measurement was calibrated by measuring the anisotropy of EGFP at different concentrations (Figure 3). As expected, the standard deviation reduces with increasing concentration and the mean value of anisotropy is independent of concentration above 10 nM. In Figure 3 (inset), the anisotropy at different viscosities (realized by mixing glycerol to the solution while keeping EGFP concentration fixed) is shown. The viscosity dependence of anisotropy is given by the Perrin equation,

$$r = \frac{r_0}{1 + \frac{t\,RT}{hV}},$$

where r is the anisotropy of the fluorophores, r_0 is the anisotropy of the immobilized fluorophores, h the viscosity of the medium, V the volume of the fluorophore molecules, t the fluorescence lifetime, R, the gas constant and T the temperature. The solid line (inset, Figure 3) shows the fit to the above equation.

In Figure 4 (inset), a schematic of the transcription reaction is shown. Transcription is a polymerization process of the nucleotides, and in our experiment the fluorescent-labelled nucleotides are incorporated into the growing polymer chain. The anisotropy of the fluorophores in the polymer would be more than that of the fluorophores attached to single nucleotides. Over time, the concentration of the free nucleotides decreases as the mRNA concentration increases due to polymerization. The anisotropy of the total solution is then given by

$$r = \sum_i r_i f_i,$$

where r_i is the anisotropy of a transcript of length i bases (single nucleotides being $i = 1$), and f_i is the fractional contribution to total fluorescence from transcripts of length i. Due to mRNA polymerization, the fractional contribution to total fluorescence from the individual fluorophores decreases as a function of time, and the contribution from polymers increases. This causes an increase in total anisotropy over time. To test this, a transcription reaction was carried out using T7 luciferase control DNA (Promega) and T7 transcription kit (Promega). (Transcription protocol: The total reaction volume is 20 µl and contains all the required ingredients (T7 RNA polymerase, r-ATP, r-UTP, r-GTP, r-CTP) for the production of the luciferase mRNA. In the 20 µl transcription reaction mixture a fraction of 1/10 of r-UTP is fluorescently labelled by mixing Alexa488-labelled r-UTP (Molecular Probes) and non labelled r-UTP. Sample well is made using an O-ring fixed onto a clean micro cover glass using paraffin. All the reagents and the sample well are made RNAse free. The control DNA concentration used for transcription is 20 ng/µl.) In Figure 4, anisotropy vs time is shown clearly depicting the polymerization process. To confirm that the observation was due to polymerization of nucleotides to mRNA, the transcription reaction was repeated in the absence of the template DNA.

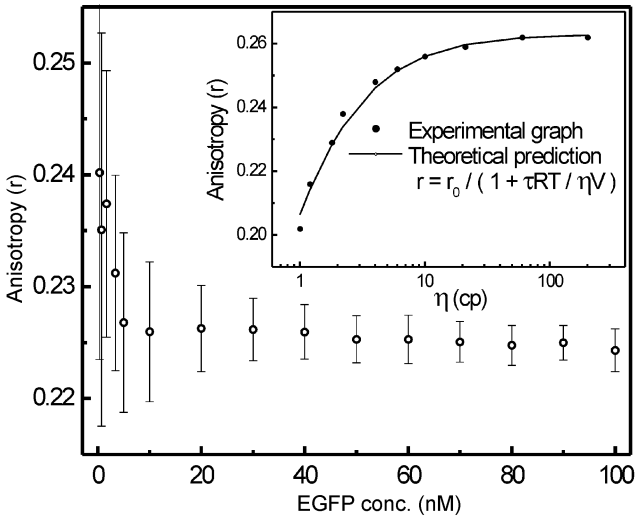

Figure 3. Concentration dependence of anisotropy. Plot of mean anisotropy and standard deviation at different concentrations of EGFP. (Inset) Plot of mean anisotropy as a function of viscosity. EGFP concentration was kept constant at 30 nM. The fit to the Perrin equation is also shown.

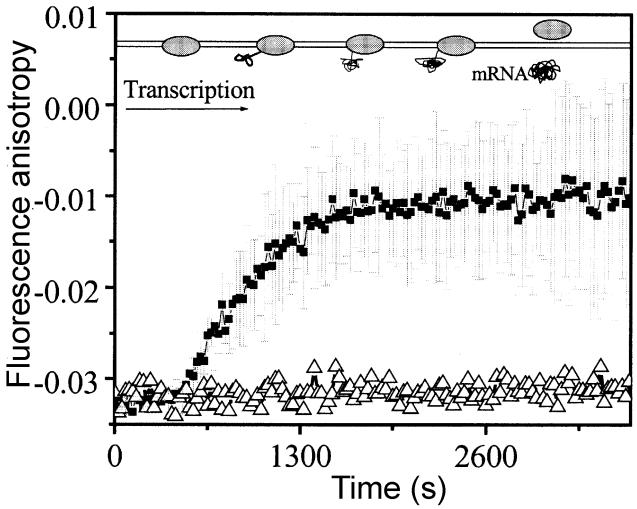

Figure 4. Plot of anisotropy as a function of time during transcription reaction. Increase in anisotropy due to polymerization of nucleotides is observed. (Inset) Cartoon of polymerization of mRNA from free nucleotides during transcription.

In the absence of DNA, no mRNA is formed, and therefore we find that the anisotropy signal remain constant.

In Figure 5, we plot the correlation function for the mRNA, EGFP and the background to compare the distinct changes in the diffusion timescales. For this the mRNA was purified and FCS was done on the transcripts. The mRNA transcripts from the transcription reaction were purified using RNeasy kit (Qiagen). The transcripts were then diluted five fold in nuclease-free water and the correlation measurement was done. The characteristic timescale of diffusion t_D is inversely proportional to the radius of the diffusing species and is obtained from the fits. As the polymerization produces mRNA of about 1700 bases length, the timescale should be of the order of a few milliseconds, which is much higher than the EGFP correlation timescales. From the plot, we calculated t_D of the mRNA to be 9 ms.

To rule out the possibility of the measurement being from an aggregation of nucleotides and not mRNA, an enzymatic digestion reaction for RNA was performed. For this 1 ng of RNAase was added to the solution and correlation was measured with time. RNAase degrades the mRNA to its monomer units. This causes a decrease in the size of the chains and therefore a decrease in the t_D values (inset, Figure 5). The plot shows clearly the decrease in t_D values, which accompany the degradation of mRNA, and finally the correlation is lost since the timescales decrease below the detection range and are masked by the noise of our equipment.

Besides the *in vitro* measurement of mRNA polymerization, we have also used the fluorescence anisotropy technique to measure *in vivo* protein–DNA interaction. The system studied is the *Escherichia coli* bacterial system, where the cells (MC4100 strain) were transformed either with plasmids coding for EGFP or EGFP–lacI fusion protein. LacI protein works as a repressor to gene-expression from lac promoter by binding to specific DNA sites. It also has strong non-specific interaction with DNA and therefore is mostly found bound to the DNA in the cell. Since anisotropy measures rotational mobility of the fluorescent species (EGFP–lacI in our case), an enhanced anisotropy is expected when the protein is bound to DNA, than when freely floating. Figure 6 shows the distribution of anisotropy measurements in cells with EGFP–lacI protein and those with only EGFP. Since EGFP–lacI is expected to bind to the DNA and therefore have slower rotational motion, its anisotropy is higher than that measured for *in vivo* free-floating EGFP. Each distribution in Figure 6 is one of anisotropy measured at a fixed point in the cell acquiring every 0.1 s for 30 s. We also find different anisotropy values at different regions of the same cell in the case of MC4100 with EGFP–lacI (data not shown). DNA-rich regions show distinctly higher values of anisotropy than the other regions, which have an almost uniform anisotropy value. In contrast, for MC4100 with EGFP there is uniform anisotropy throughout, since EGFP has no preferential affinity for DNA. Our set-up therefore has the sensitivity to pick up differential anisotropy signals *in vitro* as well as *in vivo*.

We have combined the confocal fluorescence set-up with glass micropipette (1 cm taper length and 0.5 μm tip diameter)-based force detection[4]. We present here an application to probe the unzipping forces of a condensed polytene chromosome (Figure 7). A single salivary gland cell, derived from *Drosophila* larvae, was squashed on a glass cover slip. The micropipette was coated with poly-

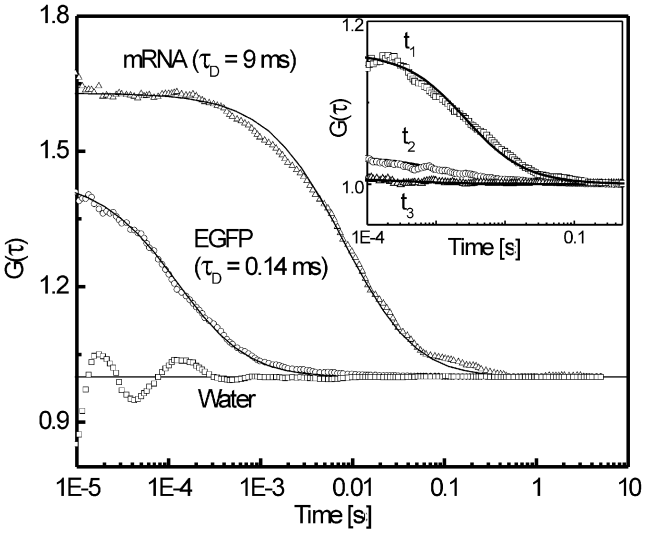

Figure 5. Plot of autocorrelation functions of water (background), EGFP and mRNA showing characteristic timescales calculated from the fits (solid lines). (Inset) Plot of autocorrelation functions of mRNA undergoing enzymatic degradation at three different time points.

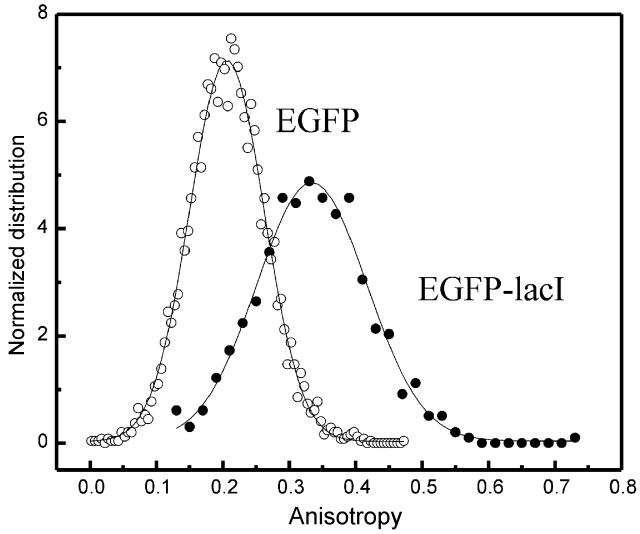

Figure 6. Distribution of anisotropy measurement on a cell with EGFP (mean ~ 0.2) and that with EGFP–lacI. Increase in anisotropy for EGFP–lacI (mean ~ 0.33) is caused by its binding to DNA.

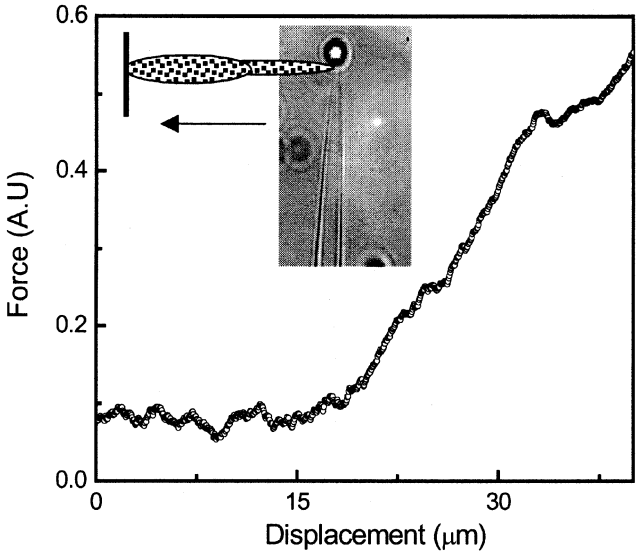

Figure 7. Force extension curve measured on a chromatin fibre. (Inset) Micropipette tip with a 2 μm bead attached to it for comparison.

L-lysine and then touched on the polytene chromosome lying on the coverslip. The chromatin fibre was then pulled from the polytene chromosome of *Drosophila* salivary gland using the micropipette. Typical force extension curves are plotted in Figure 7. The possibility to tune the structure of the chromosome using the micropipettes allow us now to simultaneously study the nucleosome dynamics using single-molecule fluorescence tracking methods.

We have constructed a confocal fluorescence measurement set-up having subnanomolar detection sensitivity with force measurement capability. The set-up is configured to study various fluorescence properties, using mainly fluorescence anisotropy, fluorescence resonance energy transfer (FRET) and FCS measurements. We have used our set-up to measure the changes in anisotropy during transcription of mRNA, and confirmed the measurement by FCS of the purified mRNA transcripts and enzymatic degradation of the transcripts. The combination of FCS, fluorescence anisotropy and FRET measurements makes our set-up ideal for ultrasensitive measurements in gene-expression studies. The multiple parameters would allow us to resolve the heterogeneity of the sample by recording the individual members of the ensemble with high time resolution. We have also extended the application of the set-up to measure protein–DNA binding inside single bacterial cells. Apart from fluorescence, the set-up also allows us to simultaneously measure and exert forces while recording fluorescence.

1. Michalet, X., Kapanidis, A. N., Laurence, T., Pinaud, F., Doose, S., Pflughoefft, M. and Weiss, S., The power and prospects of fluorescence microscopies and spectroscopies. *Annu. Rev. Biophys. Biomol. Struct.*, 2003, **32**, 161–182.
2. Jonathon, H., *Mechanics of Motor Proteins and the Cytoskeleton*, Sinauer Associates, Inc., Sunderland, Massachusetts, 2001.
3. Rigler, R. and Elson, E. S., *Fluorescence Correlation Spectroscopy Theory and Application*, Springer-Verlag, Berlin, 2001.
4. Soni, G. V., Hameed, F. M., Roopa, T. and Shivashankar, G. V., Development of an optical tweezer combined with micromanipulation of DNA and protein nanobioscience. *Curr. Sci.*, 2002, **83**, 1464–1470.
5. Meller, A. and Branton, D., Single molecule measurements of DNA transport through a nanopore. *Electrophoresis*, 2002, **16**, 2583–2591.
6. Xie, X. S. and Lu, H. P., Single-molecule enzymology. *J. Biol. Chem.*, 1999, **274**, 15967–15970.
7. Arava, Y., Wang, Y., Storey, J. D., Liu, C. L., Brown, P. O. and Herschlag, D., Genome-wide analysis of mRNA translation profiles in *Saccharomyces cerevisiae*. *Proc. Natl. Acad. Sci. USA*, 2003, **100**, 3889–3894.
8. Medina, M. A. and Schwille, P., Fluorescence correlation spectroscopy for the detection and study of single molecules in biology. *Bioessays*, 2002, **24**, 758–764.
9. Lakowicz, J. R., *Principles of Fluorescence Spectroscopy*, Plenum Press, New York, 1999, 2nd edn.

Received 18 November 2003; revised accepted 15 March 2004

Cloning and expression of AmphiSRP19, a homologue of SRP19 from amphioxus *Branchiostoma belcheri tsingtauense*

M. Liu[1], S. Zhang[1,*], Z. Liu[1], Y. Wang[1], H. Li[1] and A. Xu[2]

[1]Department of Marine Biology, Ocean University of China, Qingdao 266003, PR China
[2]College of Life Science, Zhongshan University, Guangzhou 510275, PR China

Signal recognition particle (SRP) plays a critical role in the co-translational translocation of membrane-bound and secreted proteins. An essential component of SRP is the protein SRP19, which is the initiator of the SRP assembly. An amphioxus cDNA clone, *AmphiSRP19*, encoding the protein SRP19 is isolated from the gut cDNA library of *Branchiostoma belcheri tsingtaunese*. The predicted amino acid sequence of AmphiSRP19 exhibits 52.8, 54.9, 42.3, 35.3, 28.2 and 19.7–24.6% similarity to its known counterparts from human, mouse, *Drosophila*, rice, thale cress and five fungi species respectively. Like other eukaryotic SRP19 proteins, AmphiSRP19 has the most conserved amino acid residues located at the sites required for binding to SRP RNA. Northern blotting and *in situ* hybridization analyses show that AmphiSRP19 is expressed in all the tissues examined, including notochord, gill, muscle, gut and fully-grown testes and ovaries of adult amphioxus, and in all the embryos

*For correspondence. (e-mail: zscshab@public.qd.sd.cn)